2014

Tuning and Optimization of Silk Fibroin Gels for Biomedical Applications

Michael Marin
Virginia Commonwealth University

Tuning and Optimization of Silk Fibroin Gels for Biomedical Applications

A thesis submitted in partial fulfillment of the requirements for the degree of Master of Science at Virginia Commonwealth University

by

Michael A. Marin
Director: Mark A. McHugh, PhD, Chemical and Life Science Engineering
Professor of Chemical Engineering

Virginia Commonwealth University
Richmond, Virginia
April, 2014

Acknowledgment

I would like to express gratitude to all the people who helped me complete this thesis; particularly Dr. Mark McHugh and Dr. Rajendar Mallepally who mentored me almost every day over the past two years. Without this close mentorship I would not have improved as much as I have. Furthermore, I would like to thank my undergraduate research mentors Dr. Maryanne Collinson and Dr. Balamurali Kannan for giving me the opportunity to start my research career and help me develop my research skills. I would also like to thank my other colleagues who helped me along the way including Sithara Nair, Vasudha Surampudi, Dr. Raj Rao, and Dr. Bruce Rubin, Sarah Rozycki, and Jennifer Bradley. I would also like to thank my committee members Dr. Maryanne Collinson, Dr. Raj Rao, and Dr. Mark McHugh for taking time from their busy schedules to review my thesis and attend my defense. Lastly, special thanks go to the Office of Naval Research and Virginia Commonwealth University whose support made this work possible

Table of Contents

List of Tables.

List of Figures.

Abstract

TUNING AND OPTIMIZATION OF SILK FIBROIN GELS FOR BIOMEDICAL APPLICATIONS

By Michael A. Marin

A thesis submitted in partial fulfillment of the requirements for the degree of Master of Science at Virginia Commonwealth University.

Virginia Commonwealth University, 2014.

Major Director: Dr. Mark A. McHugh, Professor of Chemical Engineering, Chemical and Life Science Engineering

Biocompatible and biodegradable porous materials based on silk fibroin (SF), a natural protein derived from the *Bombyx mori* silkworm, are being extensively investigated for use in biomedical applications including mammalian cell bioprocessing, tissue engineering, and drug delivery applications. In this work, low-pressure, gaseous CO_2 is used as an acidifying agent to fabricate SF hydrogels. This low-pressure CO_2 acidification method is compared to an acidification method using high-pressure CO_2 to demonstrate the effect of CO_2 mass transfer and pressure on SF sol-gel kinetics. The effect of SF molecular weight on the sol-gel kinetics is determined using the low-pressure CO_2 method. The results from these studies demonstrate that low-pressure CO_2 processing proves to be a facile method for synthesizing 3D SF hydrogels. We also determined the effect of SF solution concentration on the morphology and textural properties of SF aerogels. Changing the solution concentration from 2 wt% to 6 wt% yielded a higher surface area (260 to 308 m^2/g) and different macro structure, but similar mesopore pore volume and size, and micro structure. Furthermore, we determined the effect of drying method on the morphology and textural properties of SF hydrogels gelled via CO_2 acidification. Drying

with supercritical carbon dioxide ($scCO_2$) yielded an aerogel surface area five times larger than aerogels that were freeze dried. Moreover, a freeze dried hydrogel initially frozen at -20 °C had pores approximately 10 µm larger than a hydrogel initially frozen at -196 °C. The results presented here also demonstrate the potential of SF aerogels as drug delivery devices for the extended release of ibuprofen, a model drug compound. SF aerogels are loaded with ~21 wt% of ibuprofen using $scCO_2$ at 40 °C and 100 bar. Differential scanning calorimetry of the ibuprofen-loaded SF aerogels indicates that the ibuprofen is amorphous. Scanning electron microscopy and nitrogen adsorption/desorption analysis are used to investigate the morphology and textural properties. Phosphate buffer solution (PBS) soaking studies at 37 °C and pH 7.4 reveal that the SF aerogels do not swell or degrade for up to six hours. In vitro ibuprofen release in PBS at 37 °C and pH 7.4 occurs over a six-hour period when the ibuprofen is loaded in SF aerogel discs with an aspect ratio of ~1.65 $\left(\frac{\text{diameter}}{\text{thickness}}\right)$, whereas the dissolution of the same amount of pure ibuprofen occurs in 15 minutes. Furthermore, the release of ibuprofen from these SF aerogel discs are modeled using the Fu model which indicates that ibuprofen release follows Fickian diffusion for the first 65 wt% of ibuprofen release, and non-Fickian diffusion for the next 25 wt% of ibuprofen release. We also showed that SF aerogel scaffolds support *in vitro* human foreskin fibroblast cell attachment, proliferation, propagation, and cell seeding of different densities ($10x10^3$, $30x10^3$, and $60x10^3$). In summary, we created and characterized a tunable 3D SF aerogel scaffold with potential for applications in drug delivery and tissue engineering applications.

1 Introduction

1.1 Synthetic polymers as a biomaterial

Synthetic polymers have been extensively investigated for biomedical applications such as drug delivery, tissue engineering, and stem cell growth due to their reproducibility and tunability. [2, 3] However, these synthetic materials often lack biocompatibility and biodegradability which are essential for biomedical applications. [4] For example, poly(lactic-co-glycolic) acid (PLGA), is FDA approved, hydrolytically degradable, and mechanically strong; however, they are hydrophobic and usually processed under severe conditions that are not compatible for cells. [2] A viable alternative to synthetic polymers are natural polymers which have better biocompatibility and biodegradability. [5]

1.2 Silk fibroin as a biomaterial

Silks are a popular natural protein due to their attractive features such as abundancy, biocompatibility, biodegradability, excellent mechanical properties [6], mild process conditions, genetic engineerability [7], and their controllable degradation by enzymes. [8] Silk is spun by some Lepidoptera larvae such as silkworms, and other arthropods including spiders, scorpions, mites, moths, butterflies, wasps, and bees. [9] It is composed of two proteins, SF and silk sericin, which are made of amino acids glycine, alanine, and serine. [10] Silk sericin, which composes ~25 to 30 wt% of silk, is hydrophilic and has a glue-like character that holds the hydrophobic silk fibroin (SF) fibers together. [11] This protein is composed of primarily serine and smaller amounts of 18 other amino acids and only contains amorphous secondary structures. SF, composing ~70 to 75 wt% of silk, is a glycoprotein that contains equimolar subunits of 25 and 370 kDa segments that are covalently linked by disulfide bonds and contain crystalline and amorphous regions. [12, 13] SF consists of 90% glycine, alanine, serine, valine, and tyrosine

with characteristic repetitive sequences of GAGAGS, GAGAGY, and GAGAGVGY which are responsible for the formation of beta sheets. [9]

Due to beta sheet formation silks have slow degradation in vitro and in vivo when compared to collagens and many other biopolymers. [14, 15] This mechanical integrity and maintenance is necessary during tissue formation and is better in SF then other natural or synthetic polymers. [6, 16] Previously investigated forms of SF biomaterials include films [17, 18], nanofibers [19-22], scaffolds [6, 16, 23], powder [24], and hydrogels [25, 26]. Of the previously mentioned materials, hydrogels are the most widely investigated form for applications such as tissue regeneration [27, 28], cell scaffolds [29, 30], and drug delivery [3] .

1.3 Silk fibroin hydrogels, cryogels, and aerogels

Gelation of aqueous SF solution occurs through inter- and intra-molecular, physical, hydrophobic, and hydrogen bonding interactions of protein chains and are stable in the body unless exposed to enzymatic or oxidative stress. [9] Sol-gel kinetics of SF solutions can be accelerated by manipulating environmental factors such as solution pH, temperature, and addition of ions. For example, the gelation time of aqueous SF solutions at pH 6 – 7 decreases from days to hours if the pH is titrated to near the isoelectric point of SF (pH 3.8 – 4.0). [31] Although conventional mineral acids, such as H_2SO_4 or HCl, can be used to lower the pH, the rapid, nonhomogeneous drop in pH promotes the formation of a viscous gel interspersed with non-gelled solution. The resultant gel solution also requires additional downstream processing to remove the acids from the gel. Sol-gel kinetics of aqueous SF solutions are also a function of SF concentration and molecular weight. A previously published study has shown that gelation time is inversely proportional to SF concentration. [31] However, to the best of our knowledge, no study has reported on the effect of SF molecular weight on sol-gel kinetics.

Native SF, obtained from the silkworm cocoon, is a biopolymer with a molecular weight of approximately 340 kDa. Sericin, that coats SF, must be removed in a "degumming" step, although this degumming process can potentially degrade the SF chains. The degumming process, in general, occurs as raw cocoons are maintained in a solution of degumming reagent for a certain period of time. The degree of SF degradation depends on the strength of the degumming reagent, the degumming time, and the temperature of incubation. [32-35] The degumming method, which fixes the resultant SF molecular weight, has a significant effect on the gelation kinetics since the formation of a polymer gel is related to the degree of polymer chain overlap in solution, as shown pictorially in Figure 1. The chain overlap concentration, C^*, is proportional to C_p, the polymer concentration in solution, and inversely proportional to the square root of M_w, the weight-average polymer molecular weight. [36]

$$C^* = C_p \bullet M_w^{-1/2} \quad (1)$$

When the polymer concentration in solution is less than the overlap concentration the amount of chain-chain interactions is very low, whereas, at greater than the overlap concentration, the predominance of chain entanglements promotes a significant amount of chain-chain interactions. If there are no other factors effecting the mechanism of gelation, such as a significant decrease in solution pH, a viscous gel is more likely to form if the solution concentration is greater than the overlap concentration. [37]

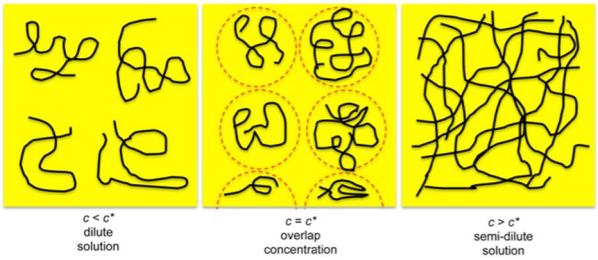

Figure 1. Schematic diagram depicting the effect of concentration on polymer chain entanglements; c - solution concentration and c^* - overlap concentration [1].

A new approach is described here for fabricating SF hydrogels using low-pressure, gaseous CO_2 as an acidifying agent. The experiments presented in this study decouple the influence of SF solution concentration from that of SF molecular weight on the observed gelation kinetics. SF hydrogels are synthesized using both low and high pressure CO_2 to demonstrate how CO_2 mass transfer rates influence gelation kinetics. Preliminary results are also presented on the synthesis of SF aerogels from hydrogels created by low and high pressure CO_2 processes.

Hydrogels exhibit unique properties such as open-pore network, structure tunability, and biocompatibility. [38] However, most hydrogels lack mechanical strength which can be a problem during handling. [39] This low mechanical strength and subsequent handling issue can be overcome by drying the hydrogels. SF hydrogels can be air dried, which results in a xerogel, freeze dried, which results in a cryogel, or supercritical carbon dioxide ($scCO_2$) dried, which results in an aerogel. Air drying, although the least complex method, causes the open-pore network of the hydrogel structure to completely collapse due to capillary forces from evaporating water. [40] Freeze drying eliminates capillary forces by removing water from the matrix by sublimation, which preserves the open-pore network. However, the formation of ice crystals during freezing of the hydrogel destroy the finer pore structure. [41] The drawbacks associated

with air drying and freeze drying are eliminated by using $scCO_2$ drying, thus preserving the initial hydrogel structure.

Tunability of these SF aerogel biomaterials are investigated by determining the effect of process parameters on the final aerogel properties. The effect of SF solution concentration and drying method on the SF aerogel textural and morphological properties are investigated using N_2 adsorption desorption, scanning electron microscopy, and compression testing. After investigation of these process parameters, the efficacy for SF aerogels for drug delivery and tissue engineering are investigated.

1.4 Silk fibroin aerogels for drug delivery

Methods for drug loading include soaking the aerogel in a liquid solution or contacting the aerogel with a gas or supercritical fluid saturated with drug. [42, 43] However, loading via soaking makes it difficult to fill small diameter pores with a liquid phase due to surface tension limitations, and an additional drying step is needed. On the other hand, using a gas phase to load the aerogel eliminates surface tension limitations and the extra drying step. Nevertheless, this type of processing can still be problematic due to very low drug solubility in the gas phase. A solution to this problem is to use a supercritical fluid (SCF) solvent which are known to have drug solubility's that are several orders of magnitude higher than traditional gaseous solvents. [44] In addition, an SCF solvent exhibits a very low viscosity and a low solid-SCF surface tension, which means that SCF solvent saturated with drug can easily penetrate small pores. Also, after loading the drug into the aerogel using an SCF solvent, the drying step is eliminated since the solvent is completely removed upon depressurization.

Aerogels loaded with drugs using supercritical fluids have been investigated in the past, but most of this research has primarily focused on silica aerogels. [45-47] These siliceous

materials lack biodegradability, which is one of the main prerequisites for drug delivery applications. Researchers have overcome this disadvantage by creating aerogels with polysaccharides [48, 49] or covalently-linked proteins [41] as the matrix for drug delivery. In this work, SF protein, from the cocoon of a Bombyx mori silkworm, is used to synthesize a hydrogel that is converted into an aerogel for use as a drug delivery carrier. It is worth noting that other researchers have synthesized SF drug delivery matrices. For more information the reader is referred to the review by Wenk et al. [50]. However, to the best of our knowledge, there is no prior work on the synthesis of SF aerogels as a drug delivery device.

In the present study, ibuprofen is used as a model drug compound that is loaded into SF aerogels using $scCO_2$. Aerogel surface area, pore size, pore volume, and the micro and macro structure of the open-pore network are determined using conventional analytical techniques. PBS absorption studies are performed to determine the amount of SF aerogel swelling and degradation. Lastly, release of ibuprofen from SF aerogels are measured and contrasted with the dissolution of pure ibuprofen to demonstrate the performance of these aerogels for controlled delivery applications.

1.5 SF aerogels for cell growth

Previously tissue engineering scaffolds have been synthesized using methodologies such as freeze drying [51-54] and salt leaching [6, 55]. In this study, we employ $scCO_2$ processing to create SF aerogels with high surface area, porosity, and good mechanical stability. Fibroblast cells are mesenchymal cells that perform the functions of tissue maintenance and repair by secreting extracellular matrix (ECM) in the connective tissue. In this study, the design of a SF scaffold is aimed towards mimicking the native three-dimensional cell environment with the cells being surrounded by supportive ECM providing the necessary mechanical support. Ongoing

research in this field shows that SF scaffolds in various forms aided in cell attachment and proliferation of fibroblast cells and other mesenchymal cells [56-59]. In the present study, we establish the biocompatibility of SF aerogel scaffolds for the first time by observing the cell morphology and attachment at three different seeding densities.

2 Materials and Methods

2.1 Materials

Bombyx mori silkworm cocoons are purchased from Aurora silk (Portland, Oregon, USA). Sodium carbonate, sodium bicarbonate, ibuprofen, and lithium bromide are purchased from Sigma Aldrich, USA. Human foreskin fibroblasts, formaldehyde, 4',6-Diamidino-2-Phenylindole, AlamarBlue, Dulbecco's Modified Eagle Medium with 4.5 g/L glucose, 2 mM L-glutamin, 1% penicillin/streptomycin, and 10% fetal bovine serum are purchased from Life Technologies. All the solvents are analytical grade and used without further purification.

2.2 Preparation of silk fibroin solutions, hydrogels, cryogels, and aerogels

Cocoon pieces are boiled in a stirred aqueous solution (1% w/v) of $NaHCO_3$ at 90 °C for 90 minutes or Na_2CO_3 at 90 °C for 60 minutes. Degummed fibers are recovered and washed with boiling water to remove the sericin protein that coats the silk fibroin (SF) protein. These fibers are stretched and dried overnight in an oven at 40 °C and are dissolved in 9.3 M aqueous LiBr solution (10% w/v) at 65 °C for four hours. The fiber-LiBr aqueous solution is cooled to 25 °C and then dialyzed (Snakeskin Dialysis Tubing, Thermo Scientific, USA, MWCO 3,500 Da) against distilled water for three days (2.5% v/v), with every day water replacement.

SF hydrogels are synthesized using three different methods; 1) low pressure CO_2 as a volatile acidifying sol gel accelerator, 2) high pressure CO_2 as a volatile acidifying sol gel

accelerator, and 3) the salt leaching method. Gelation via low pressure CO_2 is performed by bubbling CO_2 at two bar through the solution using a needle. Gelation via high pressure CO_2 is performed by pipetting SF solution (4 wt%, solution depth of 15 mm and surface area ~ $3cm^2$) into a beaker which is placed in a 300 mL stainless steel vessel, sealed, heated to 40 °C, and pressurized with CO_2 to 100 bar. After designated time periods the vessel is slowly depressurized over a period of ten minutes in all four cases. For these specific high pressure experiments, gelation is defined as the point where the solution becomes opaque and does not flow from an inverted beaker after depressurizing. Gelation via salt-leaching is performed by adding 4 g of granular NaCl (particle size 300 to 400 μm) slowly to SF solution. After adding salt, the gel is soaked in a series of water solutions over night to remove the salt.

SF hydrogels are synthesized into xerogels, alcogels, and aerogels. Xerogels are synthesized by initially freezing the hydrogel at either -40 °C or -20 °C. After which, the samples are freeze dried at sublimation conditions of -20 °C and two mbar for 18 hours. SF alcogels are synthesized by soaking hydrogels in a series of aqueous alcohol solutions of increasing alcohol concentration (20, 40, 60, and 80 wt%) for 15 minutes, followed by soaking in pure ethanol overnight. Ethanol is removed from the SF alcogel using $scCO_2$ at 40 °C and 100 bar to create the SF aerogel.

2.3 Determination of silk fibroin molecular weight

Dry SF is obtained from aqueous solutions by evaporating water at 100 °C under vacuum for ~12 hours. Both, Na_2CO_3 or $NaHCO_3$, degummed SF (2 wt%) are dissolved in 1-allyl-3-methylimidazolium chloride (AmimCl) at 90°C for two hours under vacuum. Storage, $G'(\omega)$, and loss, $G''(\omega)$, modulus of SF-AmimCl solutions are determined at 30 °C using a stress controlled rheometer (Texas Instruments, Model: AR1500ex) as a function of angular frequency,

ω, from 0.068 rad/s to 100 rad/s. The molecular weight of SF is determined by fitting the experimental viscoelastic data, $G'(\omega)$ and $G''(\omega)$, using Rouse-model as described elsewhere [34, 60]. The equations 1 to 4 are used to fit the experimental viscoelastic data

$$G' = \sum_i \left[W(M_i) \frac{\rho RT}{M_i} \sum_{p=1}^{N} \frac{\omega^2 \tau_{ip}^2}{(1+\omega^2 \tau_{ip}^2)} \right] \quad \text{Eq. (1)}$$

$$G'' = \sum_i \left[W(M_i) \frac{\rho RT}{M_i} \sum_{p=1}^{N} \frac{\omega \tau_{ip}}{(1+\omega^2 \tau_{ip}^2)} \right] \quad \text{Eq. (2)}$$

$$\tau_{ip} = \frac{6\eta_s M_i^2}{\pi^2 p^2 \rho RT} \quad \text{Eq. (3)}$$

$$W(M_i) = \left[\left(\frac{q+1}{M_w} \right)^{q+1} \Big/ q+1 \right] M_i^{\,q} \times \exp\left[-\frac{(q+1)M_i}{M_w} \right] \quad \text{Eq. (4)}$$

where ρ is the density, R is the gas constant, T is the absolute temperature, M_i and $W(M_i)$ is the molecular weight and weight fraction of the component i, respectively, η_s is the solvent viscosity, and $\tau_{i,p}$ is the Rouse relaxation time of i^{th} component p^{th} mode, and q is a constant related to the polydispersity where $M_w/M_n = (q+1)/q$. There is less than a 7% mean absolute percent deviation for calculated and measured values of $G'(\omega)$ and $G''(\omega)$ for each SF. The M_w of SF is 190 kDa for the $NaHCO_3$-degummed sample, subsequently referred to as high molecular weight SF, and the M_w of SF is 95 kDa for the Na_2CO_3-degummed sample, subsequently referred to as low molecular weight SF. Note that the values of the M_w of SF reported here are slightly higher than those reported in the literature [32, 34] due to milder degumming procedures employed, in both cases, in the present study.

2.4 Materials characterization

Aerogel morphology is determined using scanning electron microscopy (SEM) (HITACHI SU-70). The aerogels are lightly dabbed on double sided carbon tape stuck to aluminum stubs, then coated with ~10 nm of platinum via spin coating (Denton Vacuum, USA, Model: Desk V TSC).

Fourier transform infrared spectroscopy (FTIR) (Smart iTR, Thermo Fischer Scientific, Madison, WI, U.S.A.) is used for the structural characterization of SF aerogels. FTIR spectra are collected in the absorption mode as the mean of 64 scans at 4000 to 400 cm^{-1} with a spectral resolution of 4 cm^{-1}. Matsumoto et al. is used as a guide to label the different peaks. [9]

The physical state of the ibuprofen in the aerogel is determined using differential scanning calorimetry (TA instruments, Q10). The aerogel sample is heated at 10 °C/minute from 40 to 135 °C. Sample purge flow is set to 50 mL/minute, and resultant data from the first heat are analyzed using Universal Analysis 2000 software.

Ibuprofen loading in the aerogel is determined using Thermal Gravimetric Analysis (TGA) (Perkin–Elmer USA, Model Pyris 1 TGA). The furnace is continuously flushed with nitrogen gas at a flow of 3 L/hour. The aerogels are rapidly heated to 80 °C, held at this temperature for 15 minutes, and then rapidly heated to 200 °C and held for 30 minutes. In both cases the heating rate is 100 °C/minute.

Aerogel surface area, pore size, and pore volume are determined using nitrogen adsorption/desorption measurements at 77 K (Quantachrome Instruments, Nova 2200e). Approximately 50 mg of aerogel is heated at 120 °C under vacuum for two hours to dehydrate the aerogel before performing the adsorption/desorption measurements. The specific surface area of the aerogel is calculated with the multipoint Brunauer–Emmett–Teller (BET)

model in the relative pressure range of 0.05 to 0.30, and the pore size distribution is calculated with the Barrett-Joyner-Halenda (BJH) model using a desorption isotherm.

The volume change of an SF aerogel disk is determined by noting the change in the length and diameter of the disk submerged in 50 mL of well-stirred PBS at 37 °C and pH 7.4. The SF aerogel is removed from the solution for imaging and dimension measurement after one minute and 360 minutes. It is worth noting that at the conclusion of these soaking experiments, the SF aerogel samples did not exhibit any change from their original weight as determined gravimetrically.

2.5 Ibuprofen loading of silk fibroin aerogels by supercritical carbon dioxide

Ibuprofen is loaded into the aerogel using supercritical carbon dioxide ($scCO_2$) following the method reported by Shen et al. [61]. SF aerogel is first dehydrated at 100 °C under vacuum for two hours and then placed into an 80 mesh stainless steel basket that is attached to an impeller rod located in a stainless steel vessel. Excess solid ibuprofen is placed in the bottom of the vessel so that $scCO_2$ remains saturated during this loading process, which is run for two hours at 100 bar at 40 °C with stirring. Ibuprofen is expected to partition between the CO_2-rich phase and the SF-rich phase. [61, 62] The loading of ibuprofen, 20.6 ± 4.1 wt% (mean ± standard deviation, n = 3), is determined gravimetrically and is cross checked using TGA as subsequently described.

2.6 *In vitro* drug release study

A known amount of ibuprofen-loaded SF aerogel or pure ibuprofen is put into a stainless steel basket made with 80 mesh screen. The basket is fully immersed in 50 mL of well-stirred PBS at 37 °C and pH 7.4. Perfect sink conditions are maintained during the release experiments since the 50 ml of PBS remain below 10% of the 6.02 mg/mL maximum solubility of ibuprofen.

[61] Aliquots of PBS are removed at specific time intervals to quantify the release rate of ibuprofen and the same amount of fresh PBS at 37 °C is added back to the parent solution to maintain perfect sink conditions. The ibuprofen solution concentration is quantified using UV-Vis spectroscopy from the absorbance at 264 nm.

2.7 *In vitro* cell culture studies

Human foreskin fibroblast (HFF) cell propagation was determined using the following method. Aerogel scaffolds are washed with 100% ethanol and sterilized under UV light for 30 minutes. The sterile scaffolds are soaked in phosphate buffer solution (PBS) in an incubator for six to eight hours, followed by incubation in cell culture medium for three hours. HFFs are re-suspended in 50 µl of cell culture medium and added on top of the scaffold. After two hours of incubating the scaffold with the cells in media, more medium is added to maintain the initial volume. HFFs are maintained in DMEM with 4.5 g/L glucose, 2 mM L-glutamine, 1% penicillin/streptomycin, and 10% fetal bovine serum. Medium is replaced every two days and cells are routinely maintained in a controlled temperature and environment incubator at 5% CO_2 at 37°C.

Immunocytochemical staining is used to determine the spreading throughout the scaffold. Cells growing in SF aerogel are first washed with PBS, fixed with 3% formaldehyde for 15 minutes at room temperature, and washed once more with PBS. Subsequently, cells are incubated for one hour with Rhodamine Phalloidin which stains for actin filament of cells, followed by three washes with PBS. Cells are stained with a nuclear dye 4',6-Diamidino-2-Phenylindole, Dilactate (DAPI) followed by another PBS wash. Images are captured on a confocal LSM 710 Meta Zeiss microscope using the appropriate laser excitation.

Cell propagation is measured by incubating HFF seeded substrates for four hours with fresh incomplete culture medium (without serum supplement) supplemented with 10 vol% AlamarBlue®. Following incubation, 150 µL medium from each well is transferred to a 96-well microplate in triplicate. UV-Vis spectroscopy is to quantify the colorimetric response to the amount of cells by taking the absorbance 570 nm using 600 nm as the reference wavelength.

3 Results and Discussion

3.1 Effect of molecular weight and CO_2 mass transfer on sol-gel kinetics

The effect of silk fibroin (SF) molecular weight on sol-gel kinetics is determined using low and high molecular weight SF prepared by changing the strength of the degumming reagent. Figure 2 shows a pictorial representation of the results from low pressure, gaseous CO_2 processing of two SF solutions. As CO_2 at two bar pressure and 25 °C is bubbled through the solution with high molecular weight SF (4 wt%), foam is generated instantly and eventually collapses into a hydrogel. In contrast, as CO_2 at two bar pressure and 25 °C is bubbled through the solution with low molecular weight SF (4 wt%), only a small amount of foaming is observed which dissipates quickly and does not collapse into a hydrogel. In both cases, as CO_2 dissolves into the SF solution, the pH rapidly drops to approximately 4.0, which is the isoelectric point of SF. The SF solution is expected to gel when the solution pH is titrated to the isoelectric point of SF.[62] However, since gel formation is not observed for the solution with low molecular weight SF, it is conjectured this solution has not reached the overlap concentration that favors gel formation. To support this hypothesis, the low molecular weight SF solution is concentrated to ~13 wt% where it now rapidly gels when CO_2, at two bar pressure, is bubbled through the solution. The results from these experiments are consistent with those of Kaplan et al.[31, 62]

who reported that low molecular weight SF solutions gelled only after being concentrated to greater than 20 wt%. The results from the present study demonstrate that SF sol-gel kinetics are dependent on both the concentration and molecular weight of the SF in solution, in addition to solution pH.

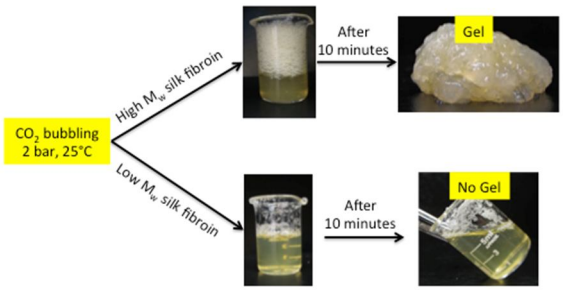

Figure 2. Effect of silk fibroin molecular weight on the sol-gel kinetics of aqueous silk fibroin (4 wt%).

Figure 3 shows the effect of CO_2 mass transfer on sol-gel kinetics by comparing the results from processing high molecular weight SF solutions (4 wt%) using CO_2 at low and high pressures. When CO_2 at two bar pressure and 25 °C is bubbled through a 5 mL SF solution, foam is generated instantly which collapses into a stable hydrogel within ~10 minutes (Figure 3a). In contrast, when high pressure CO_2 at 60 bar and 40 °C is maintained in contact with a similar, but stagnant, SF solution, it takes ~120 minutes to convert the solution into a stable hydrogel (Figure 3b). The rapid gelation time observed when CO_2 bubbles through the solution is a direct consequence of the improved rate of mass transfer of CO_2 that occurs because of the very small gas bubble-to-liquid path lengths. The enhanced uptake of CO_2 leads to a rapid titration of the pH to the isoelectric point (pH 3.8 – 4.0) of SF, which leads to quick gelation. Figure 4 confirms the rapid pH drop of distilled water when CO_2, at two bar and 25 °C, bubbles through water.

However, the pH of distilled water does not change when propane is bubbled through water indicating that there is no reaction between water and propane.

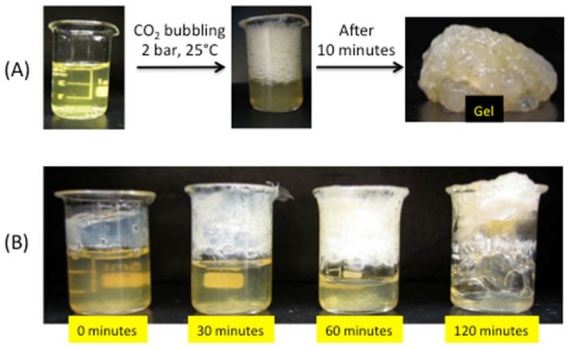

Figure 3. Impact of carbon dioxide mass transfer rate on the sol-gel kinetics of 190 kDa aqueous silk fibroin (4 wt%); (a) low-pressure, gaseous carbon dioxide at two bar and 25 °C and (b) high-pressure carbon dioxide at 60 bar and 40 °C.

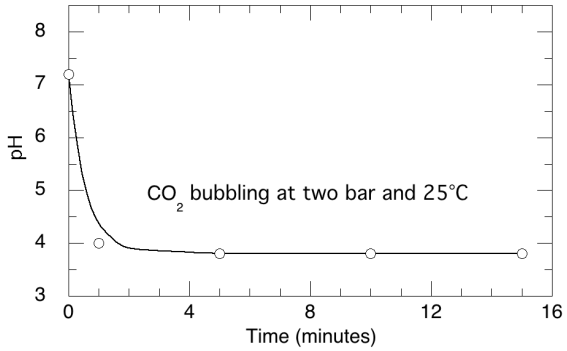

Figure 4. Change in the pH when CO_2 at two bar and 25 °C is bubbled through distilled water. The pH is measured using a double junction pH electrode (Waterproof pHTestr 20, Oakton, USA).

The very long gelation times shown in Figure 3B are a direct consequence of the slow rate of molecular diffusion of CO_2 into the stagnant solution. [63, 64] Although there is a small amount of gel deposition on the inner surfaces of the beaker at zero minutes (Figure 3B) it is

important to note that it takes up to five minutes to pressurize the solution with CO_2 and up to ten minutes to depressurize and remove the CO_2. Hence, during the pressurization/depressurization steps, a small amount of CO_2 diffuses into the surface layers of the SF solution where the local pH rapidly decreases and a thin layer of gel forms. It is apparent that a large amount of gel is created when CO_2 remains in contact with the solution for 60 and 120 minutes, which allows sufficient time for CO_2 to diffuse deeper into the SF solution. The role of CO_2 mass transfer, and the concomitant decrease in solution pH, is quite significant given that these solutions contained high molecular weight SF, likely at $C_p > C^*$, where the solutions should rapidly gel. Although CO_2 mass transfer rate, thus change in pH, can be predicted by mathematical modeling [64], no attempt is made in this study to determine the pH of SF solution–CO_2 system at high pressure, which is outside the scope of this work.

The fabrication of SF hydrogels using low-pressure, gaseous CO_2, has several advantages over the previously reported method [63] using high pressure CO_2. The low-pressure method is simple, safe, rapid, and it does not require specialty high-pressure equipment, however the fundamental principles and the underlying mechanisms of the SF sol-gel transition remain the same in both approaches.

As previously mentioned, supercritical carbon dioxide ($scCO_2$) at 40 °C and 100 bar is used to convert the SF alcogels into aerogels suitable for use as scaffolds for cell growth and as drug delivery materials. [65, 66] The FTIR spectra shown in Figure 5 is used to determine the structural characteristics of SF aerogels synthesized using CO_2 at low and high pressures. Both aerogels exhibit spectral peaks characteristic of the ß-sheet structure of SF at 1620 cm^{-1} and 1700 cm^{-1} (amide I structure) and 1525 cm^{-1} (amide II structure). Hence, the ultimate aerogel structures are expected to be very similar to one another regardless of whether low or high

pressure CO_2 was used to create the original hydrogels. Likewise, the similar FTIR spectra suggest the high pressure CO_2 used for alcogel drying is simply to remove ethanol from the alcogels and not to promote further ß-sheet formation. Furthermore, the SEM images in Figure 6 confirm that the two SF aerogels exhibit similar morphologies with highly porous structures and an interconnected network of nano-fibrils.

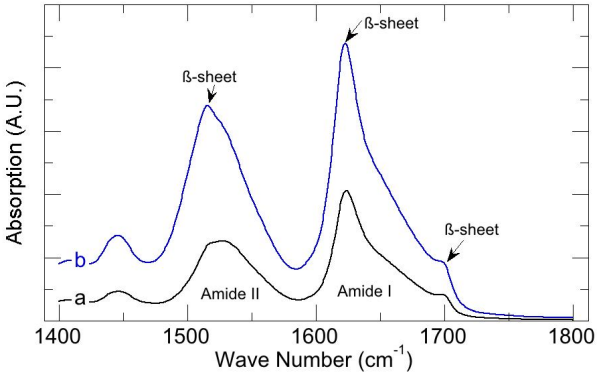

Figure 5. Fourier transform infrared spectra of silk fibroin aerogels synthesized from alcogels dried with supercritical carbon dioxide. Silk fibroin aerogels are synthesized using 190 kDa aqueous silk fibroin (4 wt%). The precursor hydrogels are created using (a) low-pressure, gaseous CO_2 at two bar and 25 °C and (b) high-pressure carbon dioxide at 60 bar and 40 °C.

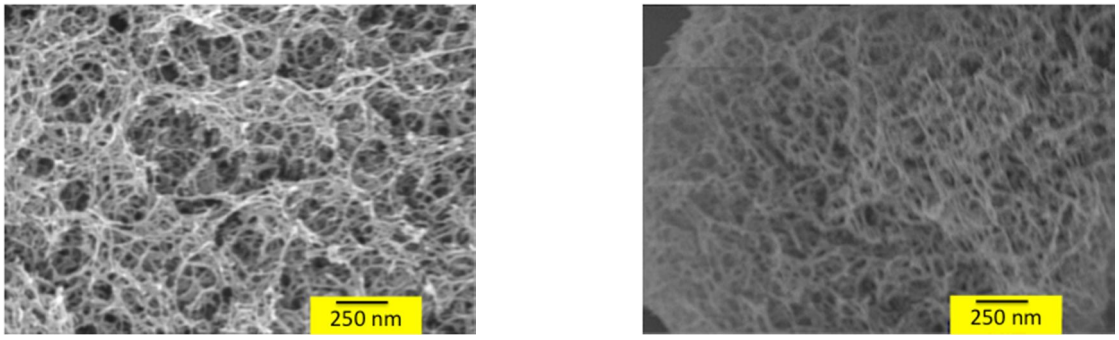

(a) (b)

Figure 6. Scanning electron microscope images of silk fibroin aerogels synthesized from 190 kDa aqueous silk fibroin (4 wt%). The precursor hydrogels are created using (a) low-pressure

gaseous carbon dioxide at two bar and 25 °C and (b) high-pressure carbon dioxide at 60 bar and 40 °C.

3.2 Effect of SF hydrogel drying techniques on final morphology

Drying method on the textural and morphological properties of SF aerogels are investigated using N_2 adsorption/desorption analysis and scanning electron microscopy (SEM). To eliminate discrepancies in hydrogel synthesis, a SF hydrogel synthesized using CO_2 as an acidifying agent is cut into three equal parts. Two parts are initially freezed at -196°C and -20 °C then freeze-dried at -20 °C and approximately two mbar pressure for 18 hours. The third part of the hydrogel is converted into an alcogel then dried using $scCO_2$.

Table 1 shows the effect of drying method on the average mesopore size and volume, as well as the total surface area. The surface area of aerogel obtained from $scCO_2$ drying (265 m^2/g) is approximately five times more than the freeze-dried aerogel (45 m^2/g). Aerogel mesopore volume obtained from $scCO_2$ drying (1.6 cc/g) is approximately an order of magnitude higher than the freeze-dried aerogel (0.05 cc/g). This is likely due to the destruction of fine porous structure during freeze drying, whereas $scCO_2$ drying preserves the fine porous structure resulting in a higher surface area and larger pore volume. Results obtained in this study are comparable to the previously reported results for whey protein aerogels [67]. The average mesopore pore sizes obtained for freeze dried aerogels using N_2 adsorption/desorption analysis ranges from two to three nm. Although, the average pore size of aerogel obtained from $scCO_2$ drying is approximately 10 nm, which is comparable to published results of other biopolymer aerogels. [67]

Table 1. Effect of drying method on the gel's average pore size and pore volume of mesopores, and total surface area. The gels are synthesized using 190 kDa aqueous silk fibroin (2 wt%).

Drying Method	**Surface Area (m^2/g)**	**Average Pore Diameter (nm)**	**Pore Volume (cc/g)**
initially frozen at -196 °C, freeze dried at -20 °C	49	3	0.05
initially frozen at -20 °C, freeze dried at -20 °C	45	2	0.04
$scCO_2$ dried	266	11	1.60

Figure 7 shows the SEM images of the aerogels obtained from the three drying methods mentioned to display the macro and micro pore size and structure. Figure 7A and 7B shows the effect of the initial freezing temperature for the freeze dried scaffolds. The aerogel in Figure 7A, which is initially frozen at -20 °C, has pores ~ten μm larger than the aerogel shown in Figure 7B, which was initially frozen at -196 °C. This is due to the larger rate of freezing that occurs when hydrogels are initially frozen at -196 °C then at -20 °C which results in the formation of different size ice crystals. From the crystallization science it is known that an increased freezing rate results in a large number of nucleation sites which inherently leads to the formation of smaller ice crystals. [68] Lastly, Figure 7C, which is an image of an aerogel obtained from $scCO_2$ drying, exhibits a distinct morphology as compared to the freeze-dried aerogels.

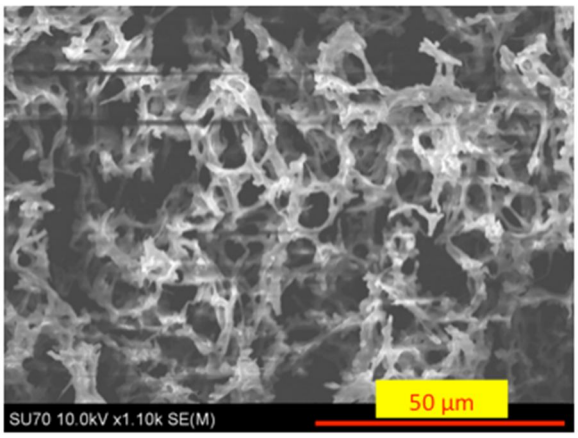

(A)

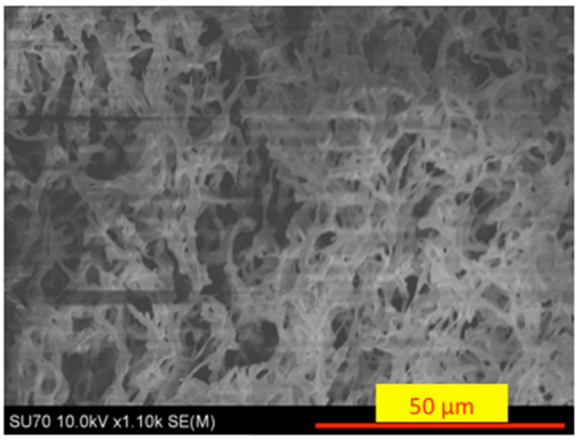

(B)

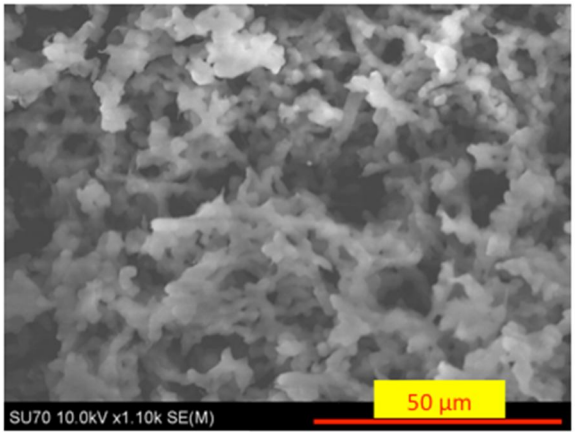

(C)

Figure 7. Effect of drying on the morphology of the silk fibroin gels synthesized from 190 kDa aqueous silk fibroin (2 wt%) (a) initial freeze at -20 °C, followed by freeze drying at -20 °C (b) initial freeze at -196 °C, followed by freeze drying at -20 °C (c) supercritical carbon dioxide drying.

3.3 Silk fibroin aerogel structural characteristics

Fourier transform infrared spectroscopy (FTIR) is used to determine the SF aerogel structural characteristics. SF is composed of amorphous random coils and crystalline β-sheet

conformations. Figure 8 shows the FTIR spectrum of a SF aerogel and air-dried SF xerogel. The infrared region 1600-1700 cm^{-1} is for amide I and 1500-1600 cm^{-1} is for amide II in the SF structural characterization. The FTIR spectra for the xerogel has random coil peaks at 1530 $cm^{-1}$and 1640 cm^{-1}in amide II and a β-sheet peak at 1525 cm^{-1}in amide I. On the other hand, the SF aerogel has β-sheet peaks at 1620 cm^{-1}, 1700 cm^{-1} in amide I, and at 1525 cm^{-1} in amide II with no observable random coil peaks. This indicates that during synthesis of a SF aerogel random coils are converted to the β-sheet conformations. This finding is congruent with other researchers and likely occurs during the formation of the SF hydrogel.

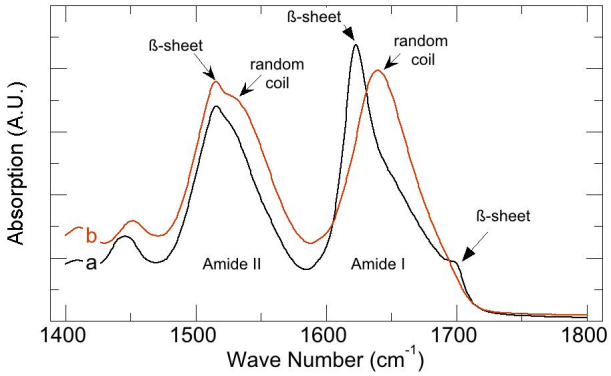

Figure 8. Fourier transform infrared spectra of silk fibroin aerogels (a) and air-dried silk fibroin xerogels (b). Gels are synthesized using 190 kDa aqueous silk fibroin (2 wt%).

3.4 Effect of silk fibroin concentration on aerogel properties

SF concentration on textural and morphological properties of aerogels are investigated using N_2 adsorption/desorption analysis and scanning electron microscopy (SEM). Figure 9 shows the N_2 adsorption/desorption isotherm of a typical SF aerogel synthesized in this study. These aerogels exhibit adsorption/desorption type IV isotherms that show a significant hysteresis indicating the presence of mesoporosity.

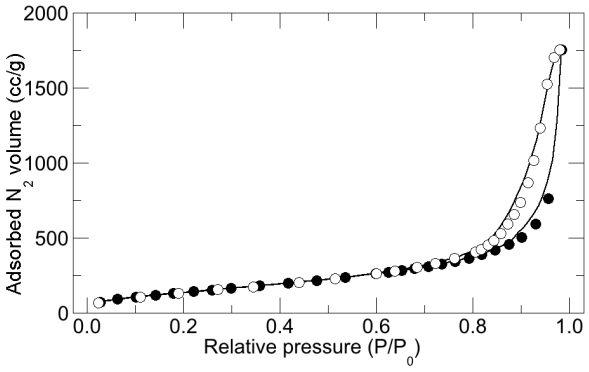

Figure 9. Typical nitrogen gas adsorption (●)/desorption (○) isotherm of silk fibroin aerogels synthesized using 190 kDa aqueous silk fibroin (2 or 6 wt%).

Table 2 shows the effect of SF solution concentration on the surface area, mesopore volume, and average mesopore diameter for the aerogel. Aerogel surface area increased from 260 to 308 m^2/g when the SF concentration increased from 2 wt% to 6 wt%, whereas mesopore volume and average mesopore diameter remained the same for both the aerogels. The increase in surface area of aerogel with increase of SF concentration is likely due to the formation of a more dense network. These results are consistent with the results reported in literature. Alnaief et al. reported that the surface area of a polysaccharide aerogel increased as the alginate concentration increased. [69]

Table 2. Effect of 190 kDa silk fibroin solution concentration (2 and 6 wt%) on the average pore size and pore volumes of mesopores, and total surface area of silk fibroin aerogels.

Concentration (wt %)	**Surface Area (m^2/g)**	**Average Pore Diameter (nm)**	**Pore Volume (cc/g)**
2	260	17	1.8
6	308	17	1.7

Figure 10 shows the SEM images of aerogel scaffolds synthesized with 2 wt% and 6 wt% SF at two magnifications to exhibit the macro and micro structure of the aerogels.

Macrostructure of both aerogels are significantly different. The aerogel made with 2 wt% SF is primarily composed of interconnected one to two µm particles (Figure 10A), whereas the aerogel made with 6 wt% SF exhibited leaf-like structure (Figure 10B). This is probably due to lower SF concentration, which initiates SF molecules to aggregate and form micron size particles which are interconnected during gelation. Whereas in highly concentrated solutions, due to enhanced intermolecular interactions, the molecules arrange in sheet-like fashion during gelation which results in a leaf-like structure. Although the macro structures were different, the microstructure of both aerogels are very similar (Figure 10C and 10D), which have a highly porous structure with an interconnected network of nano fibrils.

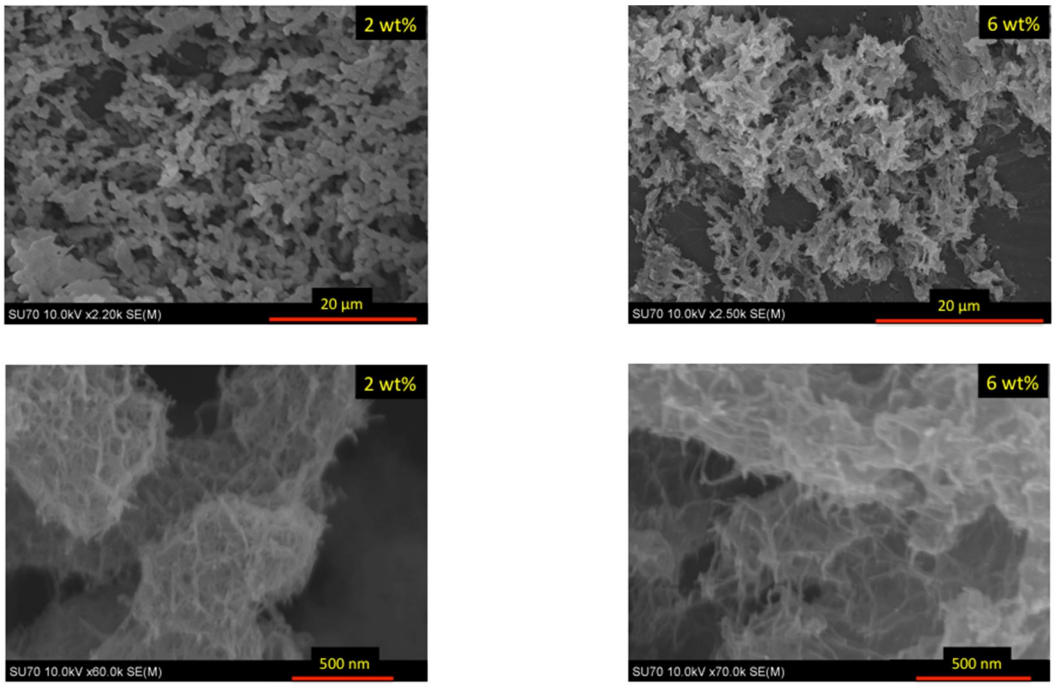

Figure 10. Scanning electron microscope images of silk fibroin aerogels at two magnifications showing the effect of silk fibroin solution concentration on the morphology of silk fibroin aerogel scaffolds. The aerogels are synthesized using 190 kDa aqueous silk fibroin (2 and 6 wt%).

3.5 Efficacy of silk fibroin aerogels for drug delivery

3.5.1 Silk fibroin aerogel characterization

Figure 11 shows a typical adsorption/desorption isotherm which is used to determine the surface area, pore size, and pore volume of SF aerogels. The isotherm exhibits type IV behavior and shows a significant hysteresis indicating the presence of mesopores. Figure 12 shows the pore size distribution of a representative SF aerogel which ranges from ~5 to 130 nm. The SF aerogels synthesized in this study have surface areas of 424 ± 75 m^2/g and densities of 0.058 ± 0.001 g/mL (mean ± standard deviation, n = 3). These SF aerogels have textural properties very similar to those exhibited by other biopolymer-based aerogels. [41]

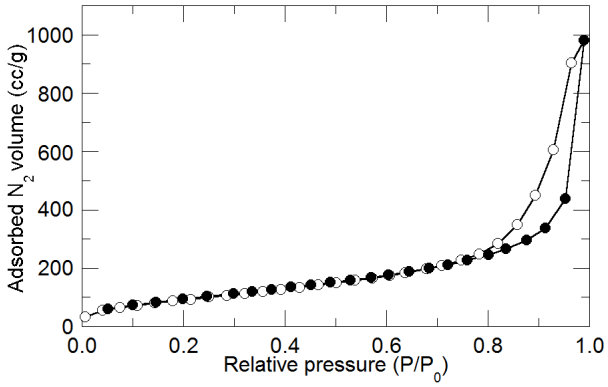

Figure 11. Typical nitrogen gas adsorption (●)/desorption (○) isotherm for silk fibroin aerogels synthesized using 95 kDa aqueous silk fibroin (4 wt%).

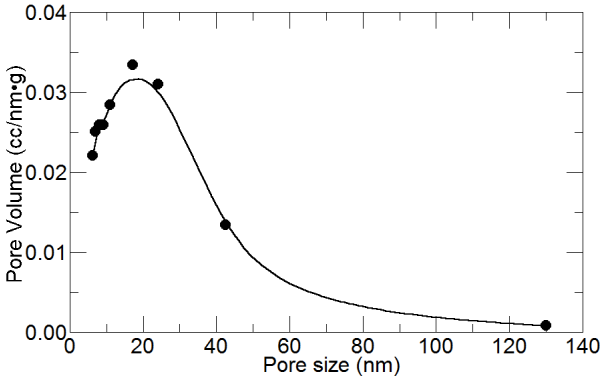

Figure 12. Typical pore size distribution of silk fibroin aerogels synthesized using 95 kDa aqueous silk fibroin (4 wt%).

DSC is used to probe the physical state of ibuprofen in the SF aerogel matrix. Figure 13 shows DSC curves for pure ibuprofen, SF aerogel, and ibuprofen-loaded SF aerogel. The pure ibuprofen curve in Figure 13a has a sharp endothermic peak at ~77 °C, which is from the melting of crystalline ibuprofen. The SF aerogel curve in Figure 14b does not contain any peaks indicating that the unloaded aerogel does not have any crystallinity. However, the curve for the SF aerogel loaded with ~19 wt% ibuprofen exhibits a small endothermic peak at ~77 °C, indicating the presence of a small amount of crystalline ibuprofen. Essentially all of the loaded ibuprofen is in an amorphous form. The results obtained in this study are consistent with the results reported by Kazarian et al. who loaded up to 30 wt% of amorphous ibuprofen into poly(vinyl pyrolidone) using $scCO_2$ assisted impregnation. [70] The results from the DSC analysis presented here suggests that the interactions between ibuprofen and the SF aerogel matrix inhibit the crystallization of ibuprofen.

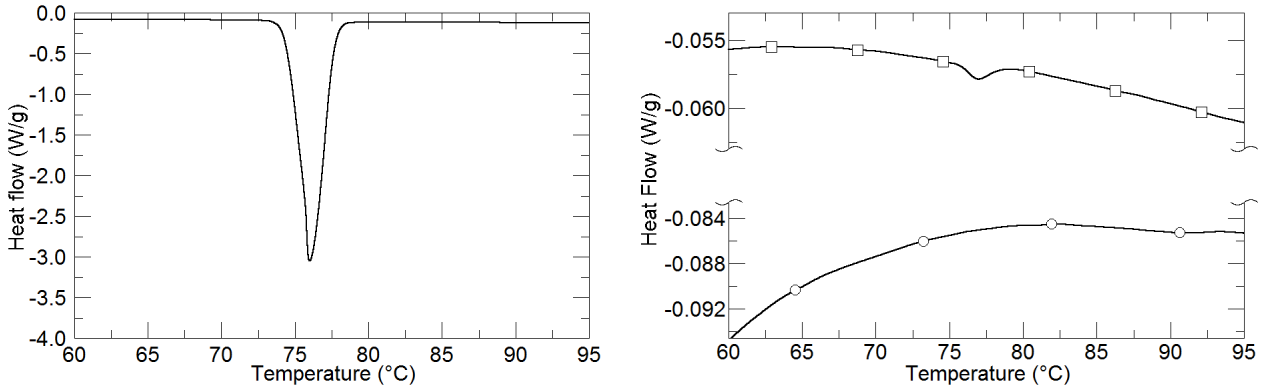

(a) (b)

Figure 13. Differential scanning calorimetry thermal curves of; (a) pure ibuprofen and (b) silk fibroin aerogel (○) and ibuprofen-loaded silk fibroin aerogel (□) obtained in this study. The aerogels are synthesized using 95 kDa aqueous silk fibroin (4 wt%). All the measurements are performed in an open pan.

Figure 14 shows the weight loss curves for pure ibuprofen, SF aerogel, and ibuprofen-loaded SF aerogel obtained by TGA. The dashed line shows the temperature profile which includes a 15 minute isothermal step at 80 ℃ to evaporate any water, followed by a 30 minute isothermal step at 200 °C to decompose and evaporate ibuprofen. SF aerogels synthesized in this study typically have 4-5 wt% of water that evaporates at 80 ℃, and another 1-2 wt% of SF degradation during the remainder of the TGA run. Figure 14 also shows that pure ibuprofen decomposes and evaporates rapidly at 200 ℃ and that the ibuprofen-loaded SF aerogel loses ~25 wt% during the 200 °C isothermal step. This weight loss is exactly matches the amount of loaded ibuprofen determined gravimetrically.

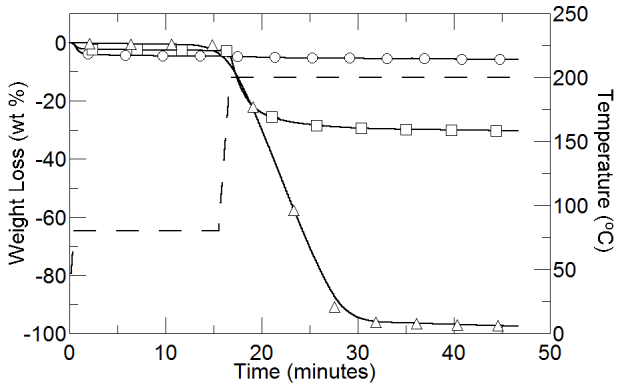

Figure 14. Weight loss curves for pure ibuprofen (△), silk fibroin aerogel (○), and ibuprofen-loaded silk fibroin aerogel (□). The aerogels are synthesized using 95 kDa aqueous silk fibroin (4 wt%). The dashed line represents the thermogravimetric analysis temperature profile.

The micro and nano structures of the SF aerogels are investigated by analyzing SEM images of representative SF aerogels and ibuprofen-loaded SF aerogels. The SEM images in Figure 15 shows the nanofibrous network of the loaded and unloaded aerogels. This fibrous network is stabilized by crystalline beta sheet conformations formed from inter- and intramolecular interactions from hydrogen bonding and hydrophobic interactions. [71] There is a strong positive correlation between the pore sizes observed in the SEM images and the pore size distribution data obtained from the N_2 adsorption/desorption analysis shown in Figure 15. It is worth noting that macroscopic ibuprofen crystals are readily apparent to the naked eye when the loading is increased above ~60 wt%. No attempt is made to determine the saturation solubility of ibuprofen in the aerogel, above which pure ibuprofen crystals are observed.

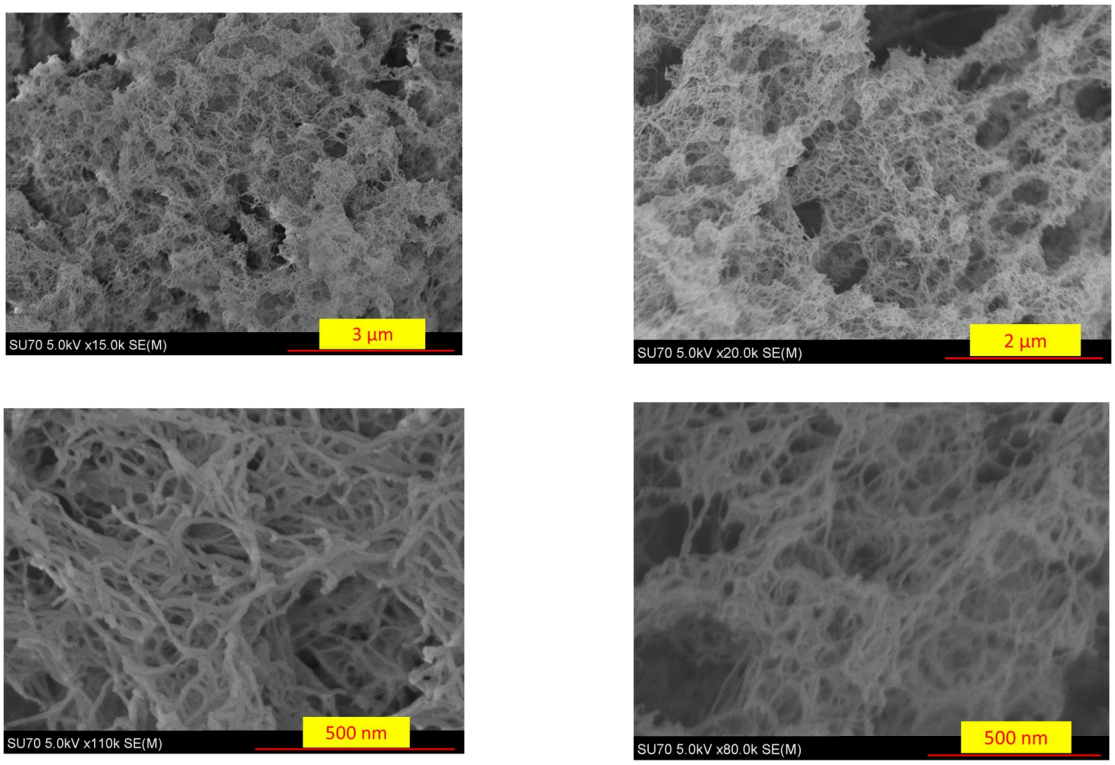

Figure 15. Scanning electron microscopy images of an unloaded silk fibroin aerogel (left column) and an silk fibroin aerogel loaded with ~21 wt% ibuprofen (right column). Each set of images are for the same sample at two different magnifications. The aerogels are synthesized using 95 kDa aqueous silk fibroin (4 wt%).

3.5.2 Silk fibroin aerogel soaking studies

Figure 16 shows images and dimensions of the SF aerogels after soaking in a well-stirring beaker containing PBS at 37 °C and pH 7.4. Initially the SF aerogel has a $\left(\frac{\text{diameter}}{\text{thickness}}\right)$ ratio of ~1.75, whereas after one minute in solution the ratio reduces ~1.65 where it remains for the next six hours. Although the $\left(\frac{\text{diameter}}{\text{thickness}}\right)$ ratio remains constant during the PBS absorption studies, the aerogel does shrink by ~46 % of its initial volume. Aerogel shrinkage in PBS at pH 7.4 could be a result of attractive ionic interactions between de-protonated carboxylic acid groups and protonated amino groups. This shrinkage behavior has been reported for other ionic

polymer hydrogels and SF microspheres in solvents with the appropriate pH. [72, 73] Further studies are in progress to further elucidate the cause behind this aerogel shrinkage. Gravimetric analysis of the dried SF aerogel revealed no aerogel degradation after soaking in PBS.

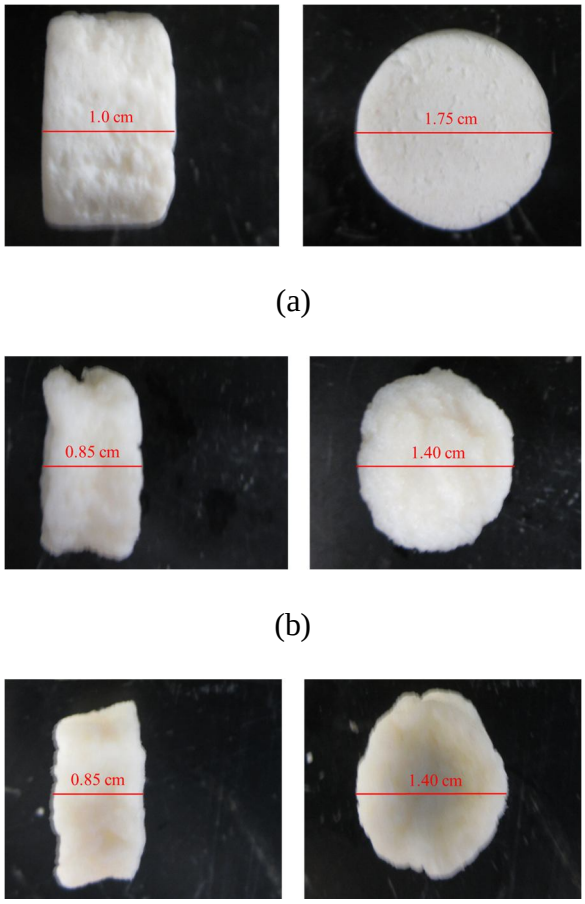

Figure 16. Side and top views of a dry silk fibroin aerogel and wet silk fibroin aerogel after soaking in phosphate buffered solution at 37 °C and pH 7.4; a) dry aerogel, b) aerogel after soaking for 1 minute, and c) aerogel after soaking for 360 minutes. The aerogel is synthesized using 95 kDa aqueous silk fibroin (4 wt%).

3.5.3 In vitro drug release studies

In vitro ibuprofen release studies are performed at perfect sink conditions to ensure there are no concentration effects on the diffusion and dissolution of ibuprofen. Figure 17 shows the release profile for pure crystalline ibuprofen powder and ibuprofen-loaded SF aerogels in PBS at 37 °C and pH 7.4. Pure crystalline ibuprofen is completely dissolved within 15 minutes, whereas ibuprofen from the SF aerogel is released over a period of approximately 360 minutes. Note that the ibuprofen loaded in the SF aerogels exhibits a release profile composed of two different rates. Initially, ~75 wt% of the ibuprofen is released in 100 minutes followed by a significantly slower release of ~15 wt% of the ibuprofen from 100 to 360 minutes. The remaining 10 wt% of the ibuprofen is either strongly bound to the SF aerogel matrix or is trapped in collapsed pores in the matrix and would not be released until degradation of the aerogel. The ibuprofen-loaded SF aerogel release profiles are similar to those observed for ibuprofen loaded alginate and eurylon starch aerogels by Mehling et al. [74].

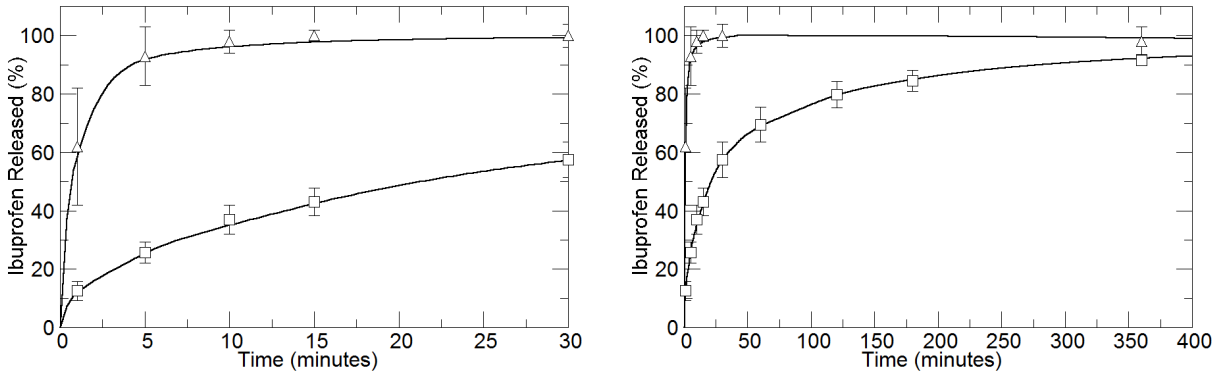

(A) (B)

Figure 17. In vitro release of pure ibuprofen (△) and ibuprofen-loaded SF aerogel (□) in well-stirred phosphate buffered solution at 37 °C and pH 7.4; A) 0 - 30 minutes and B) 0 - 400

minutes. Measurements are performed in triplicate. The aerogel is synthesized using 95 kDa aqueous silk fibroin (4 wt%).

Ibuprofen release behavior from the SF aerogels is analyzed using the model by Fu and coworkers [75], which is given by using the following three equations:

$$\frac{M(t)}{M(\infty)} = 1 - \frac{8}{l^2 a^2} \sum_{n=1}^{10} \exp(-D\alpha_m^2 t)(\alpha_m^{-2}) \sum_{n=1}^{10} \exp(-D\beta_n^2 t)(\beta_n^{-2}) \quad (1)$$

$$J_0(a\alpha_m) = 0 \quad (2)$$

$$\beta_n = \frac{(2n+1)\pi}{2l} \quad (3)$$

where M_t/M_∞ is the fractional weight release, l is the length of the aerogel, a is the radius of the aerogel, t is time, D is the diffusion coefficient of the solute, J_0 is the zero-order Bessel function, and αm are the roots of $J_0(\alpha_m)=0$. The diffusion coefficient for ibuprofen is determined by minimizing the mean average percent deviation (MAPD) between model calculations using equation 1 and the experimental data

$$MAPD = \frac{1}{n} \sum_{i=1}^{n} \frac{Experimental\ release_i - Predicted\ release_i}{Expermental\ release_i} \times 100 \quad (2)$$

where n is equal to the number of data points. An MAPD of 0.05 ± 0.005 % (mean ± standard deviation, n = 3) and a diffusion coefficient of $1.2 \times 10^{-5} \pm 3.0 \times 10^{-6}$ cm^2/s (mean ± standard deviation, n=3) is obtained when fitting the data to equation 1. This diffusion coefficient is on the order of liquid-liquid diffusion. Figure 18 shows that the release of ibuprofen from the disk shape SF aerogels suggests that the diffusion is Fickian for the first 65 wt% and non-Fickian for

next 25 wt% which is likely due to hydrogen bonding between ibuprofen and the amino acids on the SF aerogel surface.

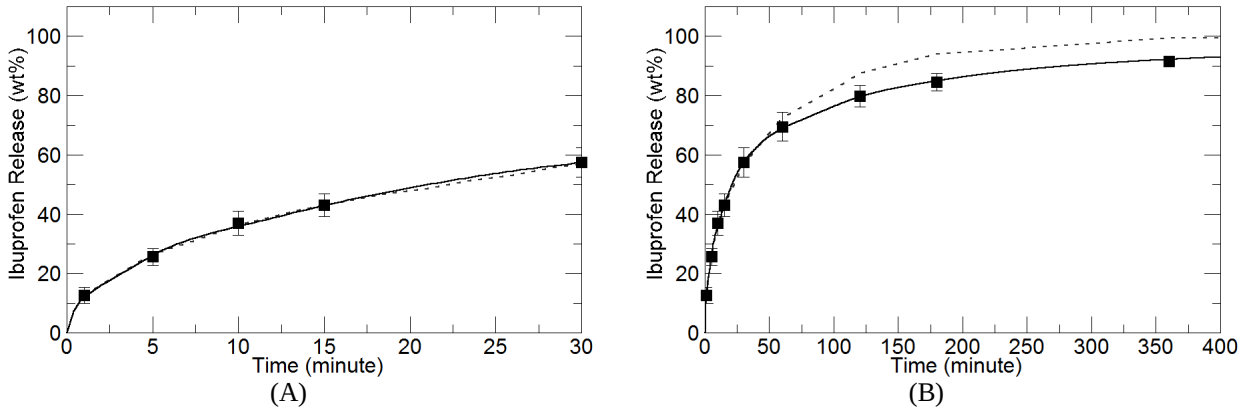

Figure 18. In vitro release of ibuprofen-loaded silk fibroin aerogel (solid line) in well-stirred phosphate buffered solution at 37 °C and pH 7.4 and Fu model fit (dashed line); A) 0 - 30 minutes and B) 0 - 400 minutes. Measurements are performed in triplicate. The aerogel is synthesized using 95 kDa aqueous silk fibroin (4 wt%).

3.6 *in vitro* cell culture studies

SF aerogel scaffolds were successful in its application for human foreskin fibroblasts (HFFs) cell attachment, propagation, cell spreading, and cell seeding of different densities ($10x10^3$, $30x10^3$, and $60x10^3$). Since SF scaffolds using the CO_2 acidification method do not have pores large enough for cells to penetrate the scaffold, we prepared scaffolds using the salt leaching method detailed in the work by Nazarov et al. [76]. Figure 19 shows the confocal microscope images from immunocytochemical analysis which revealed that there was uniform distribution of cells along the surface and layers throughout the height of the scaffold. This is an indication that there is adequate interaction between cells and polymer, which is important for biomaterials used for tissue engineering. Figure 20 shows cell proliferation across various

seeding densities of HFFs confirming the biocompatibility of the scaffold and its ability to promote cell proliferation.

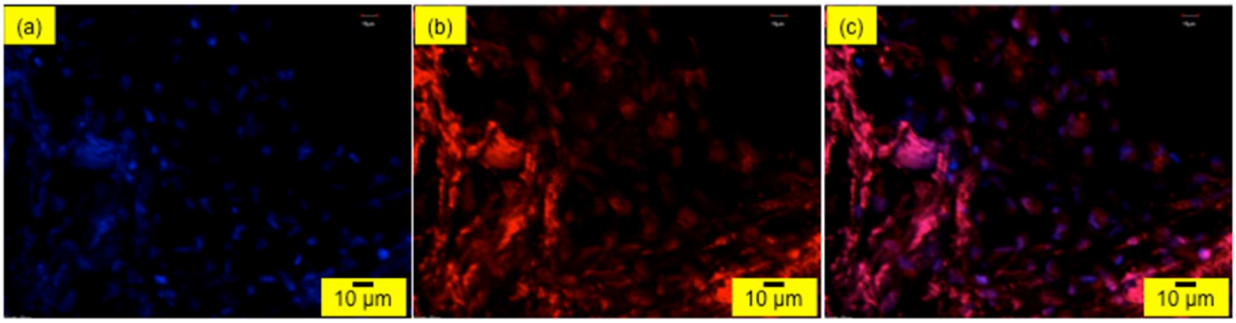

Figure 19. Human foreskin fibroblasts were cultured on the silk fibroin aerogel and after fixing, the cells were stained for nucleus using two solutions; (a) a nuclear dye, 4',6-Diamidino-2-Phenylindole, (b) an Actin protein, Rhodamine Phalloidin, and (c) is an overlaid image of (a) and (b). The aerogel is synthesized using 190 kDa aqueous silk fibroin (4 wt%)

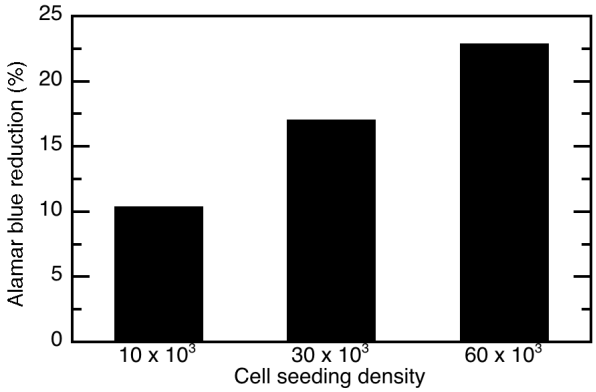

Figure 20. Comparison of the cell proliferation of human foreskin fibroblasts after 24 hours of seeding for different cell seeding density determined using the AlamarBlue® assay. The greater the AlamarBlue® reduction, the greater the level of cell growth.

4 Conclusions and Future Studies

Silk fibroin (SF) aerogel scaffolds are successfully created using sol-gel and supercritical CO_2 ($scCO_2$)processing protocols. The results presented here clearly demonstrate that SF sol-gel

kinetics are influenced strongly by both the concentration and molecular weight of SF in solution, the mass transfer rate of CO_2 into the aqueous solution, and the concomitant drop in solution pH caused by CO_2. SF hydrogels are readily synthesized using low-pressure, gaseous CO_2 at two bar with CO_2 acting as the acidifying agent. This new low-pressure, gaseous CO_2 hydrogel fabrication protocol offers a facile way to create novel materials for diverse biomedical applications.

Final aerogel textural and morphological properties of these SF aerogels are significantly affected by the SF concentration. Additionally, SF hydrogel drying method affects the pore size of final aerogel. Increasing the initial freezing rate before freeze drying reduces the pore size of the aerogel. The SF aerogels created in this study have significantly higher surface area and mesopore volume compared to the freeze-dried SF scaffolds.

The high surface area and open pore network of SF aerogels, along with their biocompatibility and biodegradability [77], make them an attractive drug delivery device. The present work demonstrates the ability of SF aerogels to deliver a model drug for an extended period of time. Ibuprofen loading using $scCO_2$ resulted in SF aerogels loaded with ~21 wt% of ibuprofen. Release of ibuprofen from SF aerogels is found to be governed by Fickian diffusion for the first 65 wt% and by non-Fickian diffusion for the last 25 wt%. Future studies should be done to demonstrate the effect of tailoring the morphological and textural properties of SF aerogels to attain a drug delivery device that yields different target drug release profiles.

SF aerogel biocompatibility is established by showing that the aerogel can support *in vitro* cell attachment, propagation, cell spreading, and cell seeding of different densities ($10x10^3$, $30x10^3$, and $60x10^3$). Future studies should be done to show time dependent cell propagation along with other related clinical applications. Furthermore, the high surface area, large mesopore

volume, and fine porous structure of SF aerogels may be useful for controlled delivery of nutrients or growth factors during cell culturing. Preliminary results also revealed that a microporous aerogel scaffold is required for human foreskin fibroblast (HFF) cell penetration. Future studies should also investigate alternative methods to prepare macroporous SF aerogel scaffolds using the CO_2 gelation method.

5 References

[1] M. Rubinstein, R.H. Colby, Polymer Physics, Oxford University Press, New York, USA, 2003.

[2] J.L. Drury, D.J. Mooney, Hydrogels for tissue engineering: scaffold design variables and applications, Biomaterials 24 (2003) 4337-4351.

[3] A.S. Hoffman, Hydrogels for biomedical applications, Advanced Drug Delivery Reviews 64 (2012) 18-23.

[4] A. Sionkowska, Current research on the blends of natural and synthetic polymers as new biomaterials: Review, Progress in Polymer Science 36 (2011) 1254-1276.

[5] C.H. Lee, A. Singla, Y. Lee, Biomedical applications of collagen, International Journal of Pharmaceutics 221 (2001) 1-22.

[6] R. Nazarov, H.-J. Jin, D.L. Kaplan, Porous 3-D Scaffolds from Regenerated Silk Fibroin, Biomacromolecules 5 (2004) 718-726.

[7] C. Wong Po Foo, D.L. Kaplan, Genetic engineering of fibrous proteins: spider dragline silk and collagen, Advanced Drug Delivery Reviews 54 (2002) 1131-1143.

[8] M. Li, M. Ogiso, N. Minoura, Enzymatic degradation behavior of porous silk fibroin sheets, Biomaterials 24 (2003) 357-365.

[9] A. Matsumoto, J. Chen, A.L. Collette, U.-J. Kim, G.H. Altman, P. Cebe, D.L. Kaplan, Mechanisms of silk fibroin sol-gel transitions, Journal of Physical Chemistry B 110 (2006) 21630-21638.

[10] S. Sundar, J. Kundu, S.C. Kundu, Biopolymeric nanoparticles, Science and Technology of Advanced Materials 11 (2010) 014104.

[11] M.N. Padamwar, A.P. Pawar, Silk sericin and its applications: a review, Journal of Scientific and Industrial Research 63 (2004) 323-329.

[12] K. Tanaka, N. Kajiyama, K. Ishikura, S. Waga, A. Kikuchi, K. Ohtomo, T. Takagi, S. Mizuno, Determination of the site of disulfide linkage between heavy and light chains of silk fibroin produced by Bombyx mori, Biochimica et Biophysica Acta (BBA) - Protein Structure and Molecular Enzymology 1432 (1999) 92-103.

[13] C.-Z. Zhou, F. Confalonieri, N. Medina, Y. Zivanovic, C. Esnault, T. Yang, M. Jacquet, J. Janin, M. Duguet, R. Perasso, Fine organization of Bombyx mori fibroin heavy chain gene, Nucleic Acids Research 28 (2000) 2413-2419.

[14] G.H. Altman, F. Diaz, C. Jakuba, T. Calabro, R.L. Horan, J. Chen, H. Lu, J. Richmond, D.L. Kaplan, Silk-based biomaterials, Biomaterials 24 (2003) 401-416.

[15] R.L. Horan, K. Antle, A.L. Collette, Y. Wang, J. Huang, J.E. Moreau, V. Volloch, D.L. Kaplan, G.H. Altman, In vitro degradation of silk fibroin, Biomaterials 26 (2005) 3385-3393.

[16] U.-J. Kim, J. Park, H. Joo Kim, M. Wada, D.L. Kaplan, Three-dimensional aqueous-derived biomaterial scaffolds from silk fibroin, Biomaterials 26 (2005) 2775-2785.

[17] B.D. Lawrence, S. Wharram, J.A. Kluge, G.G. Leisk, F.G. Omenetto, M.I. Rosenblatt, D.L. Kaplan, Effect of Hydration on Silk Film Material Properties, Macromolecular Bioscience 10 (2010) 393-403.

[18] Q. Lu, X. Wang, X. Hu, P. Cebe, F. Omenetto, D.L. Kaplan, Stabilization and release of enzymes from silk films, Macromolecular Bioscience 10 (2010) 359-368.

[19] S. Wang, Y. Zhang, H. Wang, G. Yin, Z. Dong, Fabrication and properties of the electrospun polylactide/silk fibroin-gelatin composite tubular scaffold, Biomacromolecules 10 (2009) 2240-2244.

[20] H.-J. Jin, J. Chen, V. Karageorgiou, G.H. Altman, D.L. Kaplan, Human bone marrow stromal cell responses on electrospun silk fibroin mats, Biomaterials 25 (2004) 1039-1047.

[21] C.S. Ki, J.W. Kim, J.H. Hyun, K.H. Lee, M. Hattori, D.K. Rah, Y.H. Park, Electrospun three-dimensional silk fibroin nanofibrous scaffold, Journal of Applied Polymer Science 106 (2007) 3922-3928.

[22] A.J. Meinel, K.E. Kubow, E. Klotzsch, M. Garcia-Fuentes, M.L. Smith, V. Vogel, H.P. Merkle, L. Meinel, Optimization strategies for electrospun silk fibroin tissue engineering scaffolds, Biomaterials 30 (2009) 3058-3067.

[23] Z. She, W. Liu, Q. Feng, Self-assembly model, hepatocytes attachment and inflammatory response for silk fibroin/chitosan scaffolds, Biomedical Materials 4 (2009) 045014.

[24] H. Yoshimizu, T. Asakura, Preparation and characterization of silk fibroin powder and its application to enzyme immobilization, Journal of Applied Polymer Science 40 (1990) 127-134.

[25] Z. Gong, Y. Yang, L. Huang, X. Chen, Z. Shao, Formation kinetics and fractal characteristics of regenerated silk fibroin alcogel developed from nanofibrillar network, Soft Matter 6 (2010) 1217-1223.

[26] T. Yucel, N. Kojic, G.G. Leisk, T.J. Lo, D.L. Kaplan, Non-equilibrium silk fibroin adhesives, Journal of Structural Biology 170 (2010) 406-412.

[27] C. Foss, E. Merzari, C. Migliaresi, A. Motta, Silk fibroin/hyaluronic acid 3D matrices for cartilage tissue engineering, Biomacromolecules 14 (2012) 38-47.

[28] C. Li, C. Vepari, H.-J. Jin, H.J. Kim, D.L. Kaplan, Electrospun silk-BMP-2 scaffolds for bone tissue engineering, Biomaterials 27 (2006) 3115-3124.

[29] N. Bhardwaj, S.C. Kundu, Chondrogenic differentiation of rat MSCs on porous scaffolds of silk fibroin/chitosan blends, Biomaterials 33 (2012) 2848-2857.

[30] K. Numata, T. Katashima, T. Sakai, State of water, molecular structure, and cytotoxicity of silk hydrogels, Biomacromolecules 12 (2011) 2137-2144.

[31] A. Matsumoto, J. Chen, A.L. Collette, U.-J. Kim, G.H. Altman, P. Cebe, D.L. Kaplan, Mechanisms of silk fibroin sol-gel transitions, J. Phys. Chem. B 110 (2006) 21630-21638.

[32] E.M. Pritchard, X. Hu, V. Finley, C.K. Kuo, D.L. Kaplan, Effect of silk protein processing on drug delivery from silk films, Macromol. Biosci. 13 (2013) 311-320.

[33] H. Yamada, H. Nakao, Y. Takasu, K. Tsubouchi, Preparation of undegraded native molecular fibroin solution from silkworm cocoons, Mater. Sci. Eng., C 14 (2001) 41-46.

[34] Q. Wang, Q. Chen, Y. Yang, Z. Shao, Effect of various dissolution systems on the molecular weight of regenerated silk fibroin, Biomacromolecules 14 (2013) 285-289.

[35] H.-Y. Wang, Y.-Q. Zhang, Effect of regeneration of liquid silk fibroin on its structure and characterization, Soft Matter 9 (2013) 138-145.

[36] H. Fujita, Polymer solutions, Elsevier, The Netherlands, 1997.

[37] Q. Ying, B. Chu, Overlap concentration of macromolecules in solution, Macromolecules 20 (1987) 362-366.

[38] T.R. Hoare, D.S. Kohane, Hydrogels in drug delivery: Progress and challenges, Polymer 49 (2008) 1993-2007.

[39] D.W. Hutmacher, Scaffold design and fabrication technologies for engineering tissues—state of the art and future perspectives, Journal of Biomaterials Science, Polymer Edition 12 (2001) 107-124.

[40] N. Job, A. Théry, R. Pirard, J. Marien, L. Kocon, J.-N. Rouzaud, F. Béguin, J.-P. Pirard, Carbon aerogels, cryogels and xerogels: Influence of the drying method on the textural properties of porous carbon materials, Carbon 43 (2005) 2481-2494.

[41] M. Betz, C.A. Garcia-Gonzalez, R.P. Subrahmanyam, I. Smirnova, U. Kulozik, Preparation of novel whey protein-based aerogels as drug carriers for life science applications, Journal of Supercritical Fluids 72 (2012) 111-119.

[42] P. Buisson, C. Hernandez, M. Pierre, A.C. Pierre, Encapsulation of lipases in aerogels, Journal of Non-Crystalline Solids 285 (2001) 295-302.

[43] I. Smirnova, J. Mamic, W. Arlt, Adsorption of drugs on silica aerogels, Langmuir 19 (2003) 8521-8525.

[44] M.A. McHugh, V.J. Krukonis, Supercritical fluid extraction. Principles and practice, (1986).

[45] I. Smirnova, S. Suttiruengwong, W. Arlt, Feasibility study of hydrophilic and hydrophobic silica aerogels as drug delivery systems, Journal of Non-Crystalline Solids 350 (2004) 54-60.

[46] U. Guenther, I. Smirnova, R. Neubert, Hydrophilic silica aerogels as dermal drug delivery systems–Dithranol as a model drug, European Journal of Pharmaceutics and Biopharmaceutics 69 (2008) 935-942.

[47] M. Alnaief, I. Smirnova, Effect of surface functionalization of silica aerogel on their adsorptive and release properties, Journal of Non-Crystalline Solids 356 (2010) 1644-1649.

[48] C.A. García-González, M. Alnaief, I. Smirnova, Polysaccharide-based aerogels—Promising biodegradable carriers for drug delivery systems, Carbohydrate Polymers 86 (2011) 1425-1438.

[49] T. Mehling, I. Smirnova, U. Guenther, R.H.H. Neubert, Polysaccharide-based aerogels as drug carriers, Journal of Non-Crystalline Solids 355 (2009) 2472-2479.

[50] E. Wenk, H.P. Merkle, L. Meinel, Silk fibroin as a vehicle for drug delivery applications, Journal of Controlled Release 150 (2011) 128-141.

[51] M. Garcia-Fuentes, A.J. Meinel, M. Hilbe, L. Meinel, H.P. Merkle, Silk fibroin/hyaluronan scaffolds for human mesenchymal stem cell culture in tissue engineering, Biomaterials 30 (2009) 5068-5076.

[52] B.B. Mandal, S.C. Kundu, Cell proliferation and migration in silk fibroin 3D scaffolds, Biomaterials 30 (2009) 2956-2965.

[53] Y. Wang, D.D. Rudym, A. Walsh, L. Abrahamsen, H.-J. Kim, H.S. Kim, C. Kirker-Head, D.L. Kaplan, In vivo degradation of three-dimensional silk fibroin scaffolds, Biomaterials 29 (2008) 3415-3428.

[54] J.R. Mauney, T. Nguyen, K. Gillen, C. Kirker-Head, J.M. Gimble, D.L. Kaplan, Engineering adipose-like tissue in vitro and in vivo utilizing human bone marrow and adipose-derived mesenchymal stem cells with silk fibroin 3D scaffolds, Biomaterials 28 (2007) 5280-5290.

[55] D. Yao, S. Dong, Q. Lu, X. Hu, D.L. Kaplan, B. Zhang, H. Zhu, Salt-Leached Silk Scaffolds with Tunable Mechanical Properties, Biomacromolecules 13 (2012) 3723-3729.

[56] G. Chen, P. Zhou, N. Mei, X. Chen, Z. Shao, L. Pan, C. Wu, Silk fibroin modified porous poly(epsilon-caprolactone) scaffold for human fibroblast culture in vitro, J Mater Sci Mater Med 15 (2004) 671-677.

[57] B.B. Mandal, S.C. Kundu, Cell proliferation and migration in silk fibroin 3D scaffolds, Biomaterials 30 (2009) 2956-2965.

[58] Q. Lu, X. Wang, S. Lu, M. Li, D.L. Kaplan, H. Zhu, Nanofibrous architecture of silk fibroin scaffolds prepared with a mild self-assembly process, Biomaterials 32 (2011) 1059-1067.

[59] Q. Lu, X. Zhang, X. Hu, D.L. Kaplan, Green process to prepare silk fibroin/gelatin biomaterial scaffolds, Macromol Biosci 10 (2010) 289-298.

[60] Q. Wang, Y. Yang, X. Chen, Z. Shao, Investigation of Rheological Properties and Conformation of Silk Fibroin in the Solution of AmimCl, Biomacromolecules 13 (2012) 1875-1881.

[61] Y.W. Alelyunas, J.R. Empfield, D. McCarthy, R.C. Spreen, K. Bui, L. Pelosi-Kilby, C. Shen, Experimental solubility profiling of marketed CNS drugs, exploring solubility limit of CNS discovery candidate, Bioorganic & Medicinal Chemistry Letters 20 (2010) 7312-7316.

[62] U.-J. Kim, J. Park, C. Li, H.-J. Jin, R. Valluzzi, D.L. Kaplan, Structure and Properties of Silk Hydrogels, Biomacromolecules 5 (2004) 786-792.

[63] M.L. Floren, S. Spilimbergo, A. Motta, C. Migliaresi, Carbon dioxide induced silk protein gelation for biomedical applications, Biomacromolecules 13 (2012) 2060-2072.

[64] B. Meyssami, M.O. Balaban, A.A. Teixeira, Prediction of pH in model systems pressurized with carbon dioxide, Biotechnol. Prog. 8 (1992) 149-154.

[65] M.A. Marin, R.R. Mallepally, K.R. Ward, M.A. McHugh, Silk fibroin aerogels for drug delivery applications, in, 2013.

[66] R.R. Mallepally, M.A. Marin, V. Surampudi, S. Banu, R.R. Rao, S.C. Kundu, M.A. McHugh, Silk fibroin aerogel scaffolds for mammalian cell culture, in, 2013.

[67] M. Betz, C.A. García-González, R.P. Subrahmanyam, I. Smirnova, U. Kulozik, Preparation of novel whey protein-based aerogels as drug carriers for life science applications, The Journal of Supercritical Fluids 72 (2012) 111-119.

[68] F.J. O'Brien, B.A. Harley, I.V. Yannas, L.J. Gibson, The effect of pore size on cell adhesion in collagen-GAG scaffolds, Biomaterials 26 (2005) 433-441.

[69] M. Alnaief, M.A. Alzaitoun, C.A. García-González, I. Smirnova, Preparation of biodegradable nanoporous microspherical aerogel based on alginate, Carbohydrate Polymers 84 (2011) 1011-1018.

[70] S.G. Kazarian, G.G. Martirosyan, Spectroscopy of polymer/drug formulations processed with supercritical fluids: in situ ATR–IR and Raman study of impregnation of ibuprofen into PVP, International Journal of Pharmaceutics 232 (2002) 81-90.

[71] A. Matsumoto, J. Chen, A.L. Collette, U.-J. Kim, G.H. Altman, P. Cebe, D.L. Kaplan, Mechanisms of silk fibroin sol-gel transitions, The Journal of Physical Chemistry B 110 (2006) 21630-21638.

[72] S.L. Zhou, S. Matsumoto, H.D. Tian, H. Yamane, A. Ojida, S. Kiyonaka, I. Hamachi, pH-responsive shrinkage/swelling of a supramolecular hydrogel composed of two small amphiphilic molecules, Chemistry--A European Journal 11 (2005) 1130-1136.

[73] C. Cheng, I. Teasdale, O. Brüggemann, Stimuli-responsive capsules prepared from regenerated silk fibroin microspheres, Macromolecular Bioscience (2014).

[74] T. Mehling, I. Smirnova, U. Guenther, R.H.H. Neubert, Polysaccharide-based aerogels as drug carriers, Journal of Non-Crystalline Solids 355 (2009) 2472-2479.

[75] J. Fu, C. Hagemeir, D. Moyer, E. Ng, A unified mathematical model for diffusion from drug–polymer composite tablets, Journal of Biomedical Materials Research 10 (1976) 743-758.

[76] R. Nazarov, H.-J. Jin, D.L. Kaplan, Porous 3-D Scaffolds from Regenerated Silk Fibroin, Biomacromolecules 5 (2004) 718-726.

[77] B.-M. Min, G. Lee, S.H. Kim, Y.S. Nam, T.S. Lee, W.H. Park, Electrospinning of silk fibroin nanofibers and its effect on the adhesion and spreading of normal human keratinocytes and fibroblasts in vitro, Biomaterials 25 (2004) 1289-1297.